Supporting Information for *"Production of heavily n- and p-doped CVD graphene with solution-processed redox-active metal–organic species"*

Sergio A. Paniagua,[a] Jose Baltazar,[b] Hossein Sojoudi,[c] Swagat K. Mohapatra,[a] Siyuan Zhang,[a] Clifford L. Henderson,[b] Samuel Graham,[c] Stephen Barlow,[a] and Seth R. Marder*[a]

[a] School of Chemistry and Biochemistry, Georgia Institute of Technology, Atlanta, GA 30332-0400

[b] School of Chemical and Biomolecular Engineering, Georgia Institute of Technology, Atlanta, GA 30332-0100

[c] Woodruff School of Mechanical Engineering, Georgia Institute of Technology, Atlanta, GA 30332-0405

1) Synthesis of ***2*** *and its precursor* $(NEt_4^+)_2.\mathbf{2}^{2-}$

General. All operations were performed under an atmosphere of nitrogen using standard Schlenk techniques and dry deoxygenated solvents. Compounds $\mathbf{1}^+PF_6^-$ and $\mathbf{1_2}$ were synthesised as previously described.[1-3] Compound **2** was synthesised via $(NEt_4^+)_2.\mathbf{2}^{2-}$ as described below; the starting materials $(NEt_4^+)_2.MoS_9^{2-}$ and 1,1,1,5,5,5-hexafluoropent-3-yn-2-one ($F_3CC{\equiv}CC(O)CF_3$) were synthesised according to literature methods.[4,5] All other reagents were purchased from Alfa-Aesar and used without further purification. NMR spectra were recorded on a Bruker AMX 400 MHz spectrometer. ^1H and ^{13}C chemical shifts were referenced to tetramethylsilane using the residual proton signal of the solvent and the carbon resonances of the deuterated solvent, respectively, while ^{19}F NMR spectra were referenced to $CFCl_3$ using 1,1,2-trichlorotrifluoroethane in $CDCl_3$ as an external standard. Unless stated otherwise, carbon resonances were observed as singlets. Elemental analyses were carried out by Atlantic Microlabs using a LECO 932 CHNS elemental analyzer. Mass spectra were measured on an Applied Biosystems 4700 Proteomics Analyzer.

$(NEt_4^+)_2.\mathbf{2}^{2-}$. A suspension of $(NEt_4^+)_2.MoS_9^{2-}$ (150 mg, 0.232 mmol) in CH_2Cl_2 (20 mL) was cooled to –70 °C. 1,1,1,5,5,5-Hexafluoropent-3-yn-2-one (170 g, 1.42 mmol) was added using a syringe and the reaction was stirred at –70 °C for *ca.* 3 h. The reaction mixture was then brought slowly to room temperature and stirred for 24 h. The colour of the mixture turned from red-brown to green-brown. The solution was filtered through Celite and the volatiles were removed under reduced pressure. The dark green-brown solid was extracted in hot isopropanol; the solution was filtered and cooled to –20 °C overnight. The resulting dark-green crystalline solids were washed with copious diethyl ether and then dried under vacuum (100 mg, 50%). ^1H NMR (400 MHz, CD_3CN): δ 3.156 (q, J_{HH} = 7.2 Hz, 2H, CH_2, NEt_4), 1.20 (t of 1:1:1 t, J_{HH} = 7.2 Hz, J_{HN} = ca. 2 Hz, 3H, CH_3, NEt_4). ^{19}F NMR (376.5 MHz, CD_3CN): δ –54.91 (s, CF_3), –74.03 (s, $COCF_3$). $^{13}C\{^1H\}$ NMR (100.5 Hz, CD_3CN): δ 186.88 (q, J_{CF} = 36 Hz, *C*O), 148.98 (*C*S-CO), 148.37 (q, J_{CF} = 31 Hz, *C*S-CF_3), 124.81 (q, J_{CF} = 271 Hz, *C*F_3), 117.32 (q, J_{CF} = 292 Hz, *C*F_3), 53.48 (N*C*H_2CH_3), 8.05 (NCH_2CH_3). Anal. Calcd for $C_{31}H_{40}F_{18}N_2O_3S_6Mo$: C 33.27, H 3.60, N 2.50, S 17.19, F 30.56. Found: C 33.36, H 3.45, N 2.54, S 17.04, F 30.69. MALDI-MS: *m/z* 859.9 ($\mathbf{2}^-$).

2. Excess $NOPF_6$ (155 mg, 0.89 mmol) was added to a solution of $(NEt_4^+)_2.\mathbf{2}^{2-}$ (100 mg, 0.089 mol) in CH_2Cl_2 (20 mL). The reaction mixture was stirred under nitrogen at room temperature overnight, during which time its colour turned from dark green to dark blue. The volatiles were removed under vacuum and the solid was extracted in toluene. The toluene was removed under reduced pressure and the crude dark-blue solid was dried under high vacuum. The solid was further extracted into hot hexane, filtered hot, and then slowly cooled to –20 °C overnight, to give dark blue crystals (25 mg, 33%). ^{19}F NMR (376.5 MHz, $CDCl_3$): δ –54.77 (s, CS-C*F*$_3$), –72.92 (s, CO-C*F*$_3$). $^{13}C\{^{19}F\}$ NMR (100.5 Hz, $CDCl_3$): δ 179.75 (*C*O), 169.02 (*C*S), 166.38 (*C*S), 120.27 (*C*F_3), 115.01 (*C*F_3). Anal. calcd for $C_{15}F_{18}O_3S_6Mo$: C 20.98, F 39.83, S 22.41. Found: C 21.12, F 39.64, S 22.22. EI-MS: *m/z* 859.7 ($\mathbf{2}^+$).

2) Sample preparation and characterisation

Graphene was grown on 25 μm Cu foils (Alfa Aesar, item No. 14482) using a low pressure chemical vapour deposition technique. The Cu substrates were heated up to 1000 °C in a low pressure Ar/H_2 (100/20 sccm) environment and were annealed for 30 min to increase the Cu grain size and remove any oxygen. In a typical growth step, CH_4 (35 sccm) was introduced for 15 min, and the sample was cooled to room temperature rapidly maintaining the same gas flow. The graphene samples were transferred onto bare SiO_2 substrate or prefabricated GFET devices with care taken to minimise the introduction of defects during the transfer process. During the transfer process, the Cu was etched in iron (III) chloride (30%) overnight and graphene samples were treated with hydrochloric acid (10%) for 10 min, followed by washing in deionised water to remove contaminants on the graphene film.[6] For GFET fabrication, the source and drain contacts (gold 50 nm/ chromium 2 nm thick) were defined using conventional photolithography and lift-off processes on a highly p-doped Si substrate with a 300 nm thick SiO_2 layer to create back-gated field effect transistor structures. The resulted channel size was 10 μm × 2 mm. GFET devices were measured using a probe station equipped with a HP 4156 semiconductor parameter analyser under a nitrogen atmosphere.

Toluene was purified in a MBRAUN solvent purification system with moisture absorbing filters, and additionally dried over CaH_2 or sodium/benzophenone, distilled and subjected to three freeze-pump-thaw cycles. Dissolution of the compounds, treatment of the graphene samples and GFET measurements were carried out inside a Unilab MBRAUN glovebox (< 0.1 ppm of water, < 5 ppm oxygen. Samples were typically annealed in the glovebox at 200°C for a few minutes to removed physisorbed species until the neutrality point was zero. Glassware was heated in an oven at 140 °C for at least 30 min and brought into the glovebox while hot. After treatment of the graphene films in vials or bottles, samples were rinsed in fresh toluene 3-times with shaking to remove physisorbed materials, and dried out with N_2 from a rubber bulb. The GFET with the pristine graphene in Figure 2 had an I_{DS} at minimum σ of 1.3 mA, and output characteristics were linear before and after doping for all samples.

Transfers from the glovebox into the photoelectron spectrometer were done under N_2 atmosphere using a Kratos air-sensitive transporter 39-322 that couples into the transfer chamber of our Kratos Axis Ultra^{DLD} XPS/UPS system under positive N_2 pressure. All samples were in electronic equilibrium with the spectrometer via a metallic clip on the graphene and characterisations were performed at normal take-off angle. XPS using monochromatic Al Kα line was run at a base pressure of 10^{-9} Torr with the Fermi level calibrated using atomically clean silver. Spot size was *ca.* 700 μm. Survey XPS scans were run at 160 eV pass energy and high resolution scans typically at 20 eV pass energy and 100 meV steps, while UPS was acquired at 5 eV pass energy and 0.05 eV step size with the aperture and iris set to 55 μm . Calibration of spectra of thick $\mathbf{1_2}$ (which needed charge neutralisation) was done with the Si 2p peak set to BE = 104.9 eV, same as that of the treated graphene (10 min) on silica. XPS peak fits were done with

Vision Processing Software 2.2.8 using mixed Gaussian/Lorentzian distributions to minimize *chi* squared.

UV/Visible spectroscopy was acquired in an Agilent Cary 5000 UV/Vis spectrometer for 0.5 cm radius spots (under air). Glass was used as the sample and reference to calibrate the 100%T, and 0%T was calibrated by blocking the sample light path. CVD graphene was transferred to the same type of glass slides and annealed in the glovebox at 200°C before treatment.

Raman spectroscopy was acquired in a Renishaw InVia microscope spectrometer with laser excitation at 532 nm and collection in backscattering configuration with a laser power below 0.5 mW to avoid laser-induced heating of the samples. A 50× objective lens was used to focus the laser on the graphene samples during the Raman measurements. For all of the Raman measurements, the samples were placed in N_2-filled glovebox inside a sealed microscope stage (Linkam TS 1500) to avoid air exposure during transfer and measurements.[7] The stage was mounted onto an X-Y-Z micropositioning stage to control focusing and the measurement position. A quartz window was used to allow optical access to the sample during the measurements. All Raman peaks were fitted with Gauss-Lorentzian line shapes to determine the peak position, linewidth, and intensity of the 2D and G Raman peaks.

3) Estimation of ionisation potentials

The electrochemical potential of the $\mathbf{1}^+/\mathbf{1}$ couple is –2.06 V vs. ferrocenium/ferrocene in THF/0.1 M nBu_4PF_6.[3] A solid-state IP of 3.3 V has been measured using UPS for decamethylcobaltocene[8] which is oxidized at –1.86 V in the same solvent.[9] Assuming similar solid-state polarization effects and solution solvation effects for these two systems, one would then estimate an IP of ca. 3.1 eV for **1**. A somewhat lower estimate of 2.7 eV would be obtained based on the IP of 4.8 eV reported for a bis(biphenyl) derivative of ferrocene (for which the oxidation potential is 0.00 V).[10] The IP of the unmethylated rhodocene dimer (irreversible oxidation potential E_{ox} = –0.75 V at 50 mV s^{-1}) has been measured as ca. 4.0 eV; the IP of $\mathbf{1_2}$ (E_{ox} = -0.95 V) is therefore likely to be ca. 3.8 eV.

4) Modelling of n-dopant´s footprint and estimation of surface coverage

We can estimate how many dopant monomers (**1**) can fit in a close-pack arrangement to determine an expected $Rh/C_{graphene}$ for a monolayer and compare with the obtained ratio from XPS. Figure S1c shows an estimation of molecular footprint considering the van der Waals radius for carbon and crystallographic data from $(RhCp^*Cp)^+PF_6^-$.[11] An average molecular radius of 4.6 Å is obtained (from which the footprint can be calculated to be 66 $Å^2$), but we must consider the (optimal) hexagonal close packing of discs. The unit cell can be viewed as a

rhombus (defined by green traces in Figure S1c), and its area calculated to be 73 Å^2. By comparison with graphene, for which the unit cell encompassing 2 carbons is 5.24 Å^2 (2.62 Å^2 / C), we can estimate that 3.6 molecules of **1** fit on top of 100 carbon atoms in single layer graphene; since each monomer **1** has one Rh atom, then $\frac{Rh}{C_{graphene}} = 0.036$.

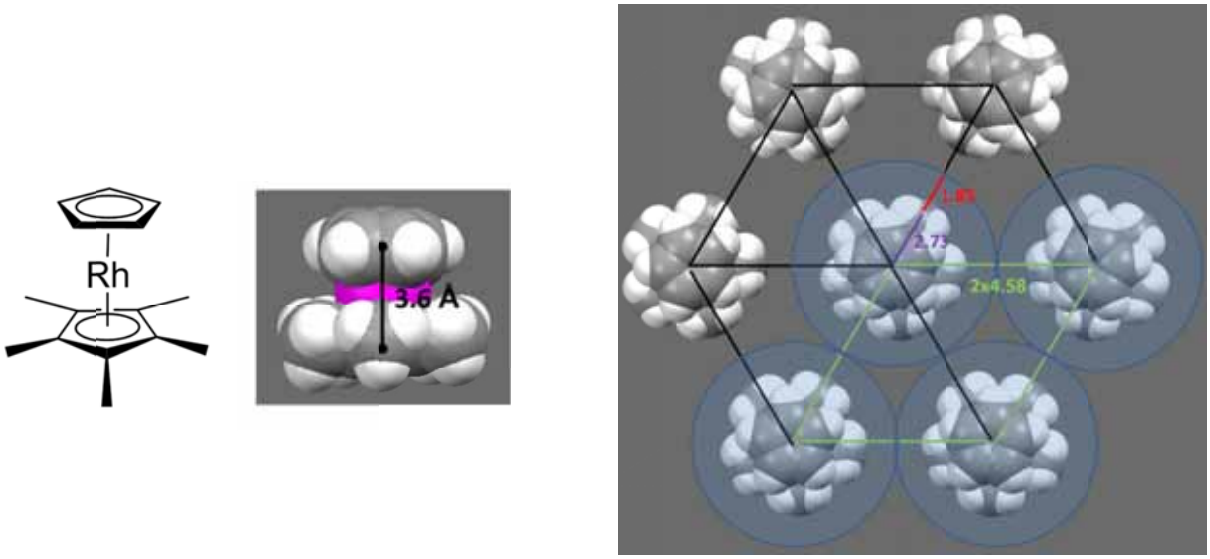

(a) (b) (c)

Fig S1 (a) Chemical structure and (b) space-filling model of **1** (monomer of $\mathbf{1_2}$). Molecular height estimated from crystallography of $(RhCp^*Cp)^+PF_6^-$, from Cp* centroid to Cp centroid. (c) Top view of a close packed model for monolayer of RhCp*Cp treating the molecules as circular discs. Cp* centroid to C from methyl group (the atom furthest from the Cp* plane) is 2.73 Å. A van der Waals radius of non-bonded C of 1.85 Å was considered.[12] The sum of the disc areas inside the rhombus defined by green lines is 91% that of the rhombus.

The C/Rh ratio from XPS corrected for the C from the dopant itself (which has a ratio of $\frac{C_{dopant}}{Rh} = 15$) can be used to estimate the experimental Rh/$C_{graphene}$ as follows.

$$\frac{C}{Rh} = \frac{C_{dopant}}{Rh} + \frac{C_{graphene}}{Rh} = 15 + \frac{C_{graphene}}{Rh} \qquad \text{Equation S1}$$

Solving for $\frac{C_{graphene}}{Rh}$ and inverting gives Equation S2:

$$\frac{Rh}{C_{graphene}} = (\frac{C}{Rh} - 15)^{-1} \qquad \text{Equation S2}$$

We can then compare the theoretical monolayer coverage of **1** on single layer graphene with the experimental from XPS, as summarised in Table SI.

5) Summary of XPS/UPS data with successive n-dopant treatments

Table SI Summary of GFET, XPS and UPS characterization after treatments with dopant $\mathbf{1_2}$. Error bars are 1σ.

Result after treatment with $\mathbf{1_2}$/**1**	*1 s in 0.025 mM*	*10 s in 2.5 mM*	*10 min in 2.5 mM*
% Close-packed ML (XPS)	2.9 ± 0.3	25 ± 1	75 ± 2
$\varphi_{treated} - \varphi_{pristine}$ */eV (UPS SEE)*	-0.26 ± 0.09	-0.67 ± 0.10	-1.28 ± 0.10
E_D-E_F*/eV (UPS VB)*	-0.20 ± 0.05	-0.50 ± 0.05	-0.70 ± 0.05
n calculated from E_D-E_F */* cm^{-2}	(4 ± 1) x 10^{12}	(2.6 ± 0.4) x 10^{13}	(5.2 ± 0.5) x 10^{13}
Electrons transferred per adsorbed dopant (UPS+XPS)	1.1 ± 0.4	0.75 ± 0.10	0.49 ± 0.05
$[Rh^{III}]/([Rh^{I}]+[Rh^{III}])$ *(XPS)*	1.0	0.81 ± 0.01	0.71 ± 0.01

6) Additional XPS, GFET, and UV/Vis data for successive treatments with n-dopant

The BE of the Si 2p and O 1s core ionisations also track linearly the change observed in the UPS valence band, consistent with the Dirac point shifting relative to the Fermi level of graphene (since the whole system is grounded through graphene, if affects the substrate peaks). The graphene C 1s peak should experience the same increase in BE, but since the dopant also contains a significant amount of carbon (at a different BE) we observed not only shifting but also the appearance of a new component leading to broadening at high coverages.

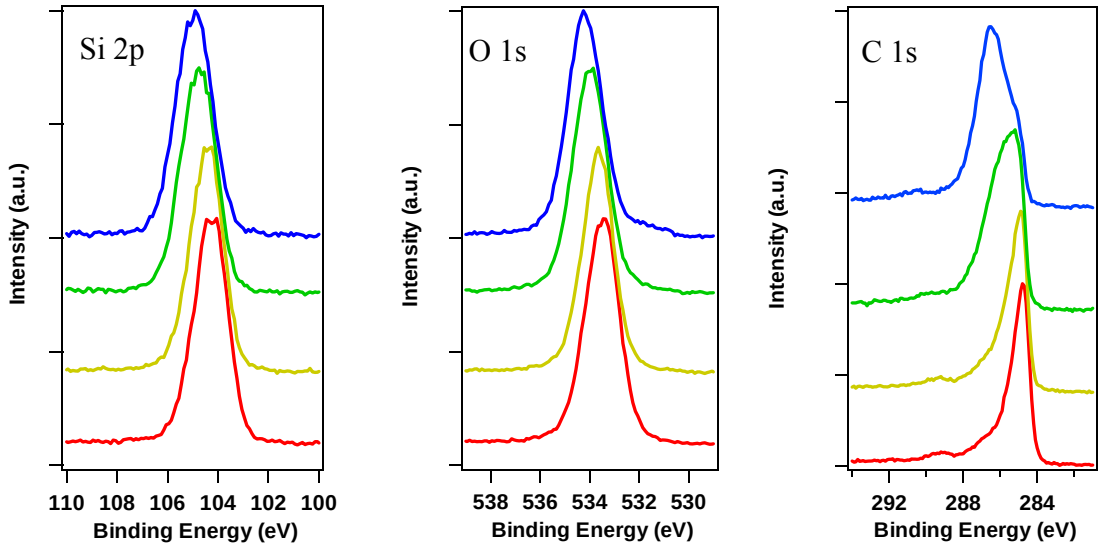

Fig S2 XPS high resolution spectra for pristine graphene (red) and after quick dip in 0.025 mM n-dopant solution (yellow), 10 s in 2.5 mM (green) and 10 min in 2.5 mM (blue). Plots offset vertically for clarity.

Table SII Binding energies (in eV) of main peaks in graphene treated with n-dopant $\mathbf{1_2}$.

Treatment	*C 1s*	*Rh^{III} $3d_{5/2}$*	*Rh^{III} $3d_{5/2}$*	*Si 2p*	*O 1s*
Pristine	284.8	-	-	104.2	533.4
Quick dip 0.025 mM	285	310.8	-	104.4	533.6
10 s, 2.5 mM	285.4	311.0	309.4	104.7	533.8
10 min 2.5 mM	286.5	311.2	309.7	104.9	534.1

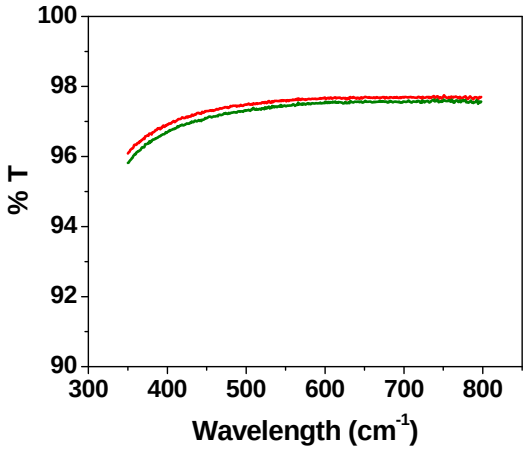

Fig S3 UV/Vis spectroscopy for graphene on glass before (red) and after treatment (green) with $\mathbf{1_2}$ 2.5 mM for 10 s.

A control experiment with $Rh^{III}Cp^*CpPF_6$ salt was carried consisting of deposition on pristine graphene to check if it changed the neutrality point. Neither dipping nor dropcasting changed the neutrality point significantly, as shown in Figure S4. We also tested dipping the samples in pure toluene, and no change in neutrality point was observed.

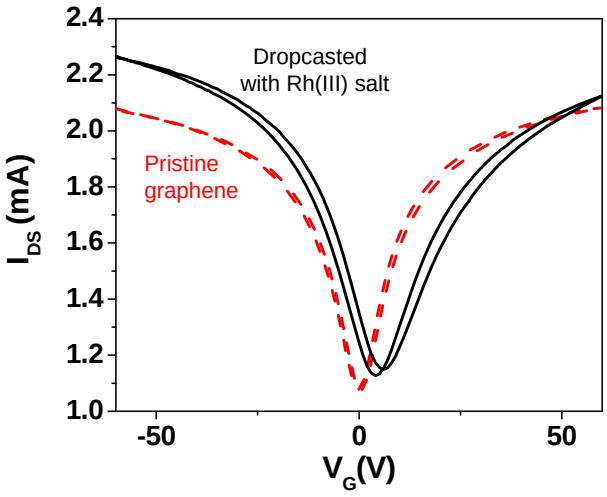

Fig S4 Transfer characteristics of graphene before and after dropcasting $Rh^{III}Cp^*CpPF_6$.

7) Contribution of surface dipole to work function change after n-dopant treatment

In the main text we referred to Equation 3 to explain the additional work function change.

$$\Delta\varphi = \Delta\varphi_{ET} + \Delta\varphi_{SD} = \hbar v_F \sqrt{n\pi} + \frac{n}{\varepsilon_0}\int_0^z \frac{q(z)}{\varepsilon_r(z)}dz \qquad Eq\ 3$$

In Figure S5 we have assumed point charges with the negative charge at the graphene plane separated from the positive charge residing on the Rh atom at 2 vdW radii[12] apart + half the molecular length. Considering an average $\epsilon_r = 10$, the estimated surface dipole from Equation 3 in the main text reproduces fairly well the observed surface dipole for a given *n*. Note that in this treatment the effective relative dielectric is assumed constant, and, therefore, also depolarization effects, are independent of coverage.[13]

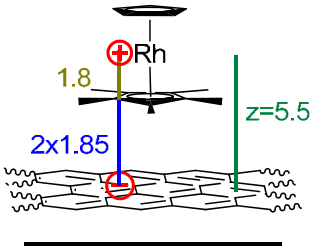

Fig S5 Schematic representation of surface dipole from electron transfer by **1**.

Table SII Estimation of surface dipole $\Delta\varphi_{SD}$ after treatment with n-dopant. Electron transfer contribution to work function change ($\Delta\varphi_{ET}$), from which *n* was determined, is shown as well.

Treatment	*Observed* $\Delta\phi_{ET}$ *(eV)*	*n from* $\Delta\phi_{ET}$ / 10^{13}	*Inferred* $\Delta\varphi_{SD}$ *(eV)*	μ_{SD} =q×z *(C*m)*	*Estimated* $\Delta\varphi_{SD}$ *(eV)*
Quick dip	-0.20 ± 0.05	0.4	-0.06 ± 0.10	1.3×10^{-28}	-0.04
10 s 2.5 mM	-0.50 ± 0.05	2.6	-0.17 ± 0.12	5.4×10^{-29}	-0.26
10 min 2.5 mM	-0.71 ± 0.05	5.2	-0.59 ± 0.11	1.0×10^{-28}	-0.51

8) Full Raman spectra for successive n-dopant treatments

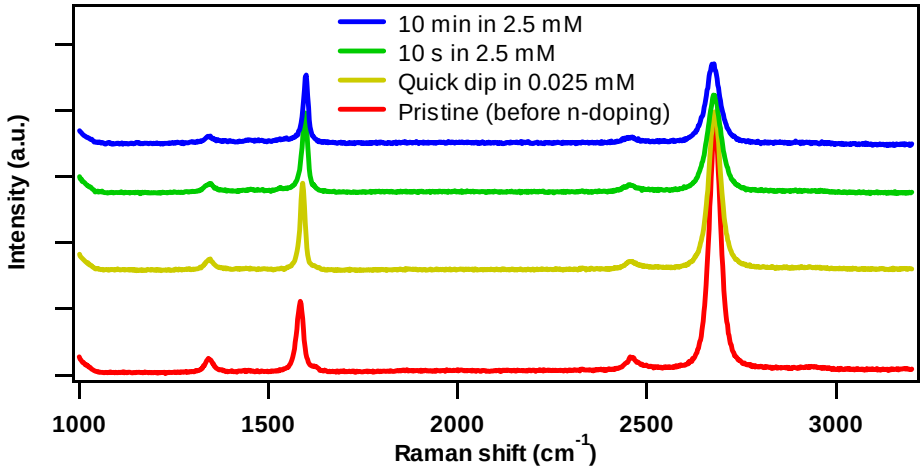

Fig S6 Raman spectra for graphene before and after successive n-doping treatments. Plots offset vertically for clarity.

9) Modeling of p-dopant´s footprint and estimation of surface coverage

A similar approach to that of section (4) can be used for the p-dopant, but in this case given the geometry of the molecule, we can consider it triangular, with alternated close-packing. The area of each triangle comes to 81 Å^2. Knowing the F/C ratio for the dopant is 18/15, we can estimate the $F_{dopant}/C_{graphene}$ from Equation S3 derived in the same way as Equation S2, and finally determine the dopant coverage by accounting for the 18 fluorine atoms per dopant as in Equation S4. For the graphene sample used in the p-doping systematic study discussed in the paper, we noticed the C content for the pristine sample was 30% higher than the usual single layer graphene, so the C area was corrected to account for that excess of carbon in our coverage determination.

$$\frac{F}{C_{graphene}} = \left(\frac{C}{F} - \frac{15}{18}\right)^{-1} \qquad \text{Equation S3}$$

$$\frac{Dopant}{C_{graphene}} = \left(\frac{F}{C_{graphene}}\right)/18 \qquad \text{Equation S4}$$

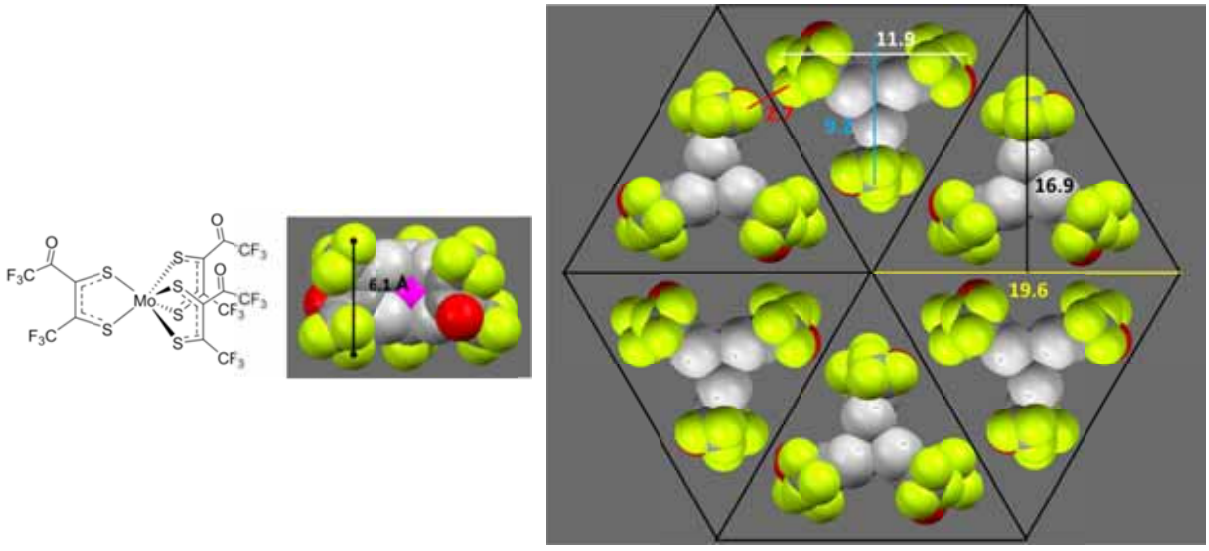

(a) (b) (c)

Fig S7 (a) Chemical structure and (b) space-filling model of **2**. Molecular height estimated from crystallography defining planes from the F atoms at the edges of the molecule. (c) Top view of a close packed model for monolayer of **2** treating the molecules as triangles. Molecular lengths are estimated from planes using the outermost F atoms, which give 11.9 Å on the x axis (white) and 9.2 in the y axis (light blue). A closest separation of the van der Waals radius of non-bonded F of 1.35 Å was considered ($2\times R_{vdW}$ = 2.7 Å in red).[12] This defines triangles of 19.6 Å of base and 16.9 Å height, for an effective footprint of 166 Å^2.

10) Summary of GFET, XPS, and UPS data with successive p-dopant treatment

Figure S8 shows the GFET results after successive treatments on graphene. As with the n-dopant, the increase in conductivity seems to be limited by the intrinsic on/off ratio of the pristine graphene, as further treatments with more concentrated solutions and for more extended periods of time give an increase in conductivity of 2.2×, not much more beyond the original 1.8× increase after the quick dips. From the observed V_{NP} after two quick dips in 0.05 mM solution, a hole density of 4.3×10^{12} cm^{-2} is calculated according to Equation 1. Additional immersion times and higher concentrations give neutrality points outside the measureable range.

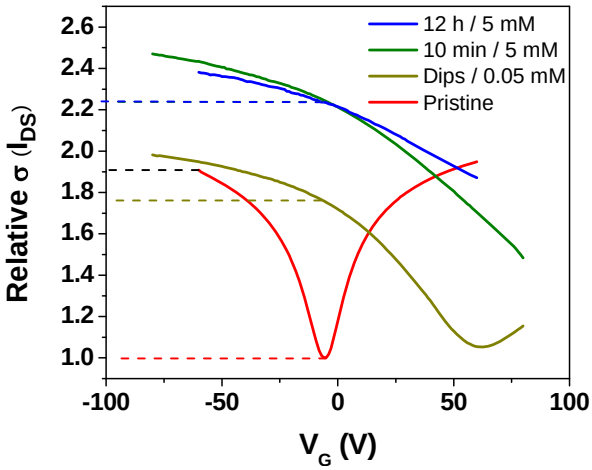

Fig S8 GFET transfer characteristics before and after treatment with **2**. Initial on/off ratio (black dash) and relative increases in current at V_G~0 are shown (V_{DS} = 0.1 V).

XPS reveals increasing surface concentrations of F, Mo, and S as treatment time increases (Figure S9a-c). We estimated from XPS F/C ratios the dopant's surface concentrations as 6%, 26% and 54% after quick dips in dilute toluene solution, 10 min and overnight immersion in 5 mM respectively. Figure S9c follows the evolution of the C 1s signal, where the appearance of a C-F component from the dopant around 293 eV is noticeable after 10 min and is much better observed after overnight treatment. Removing electrons from the valence band through p-doping will shift the main graphene C1s peak to lower binding energies since the Fermi level is being lowered relative to the Dirac point.[14] Given the contribution from the dopant to the main C 1s peak is negligible, we have calculated the induced hole density from the difference in binding energies with respect to that of pristine graphene, and the results are shown in conjunction with the UPS data in Table SIII. Figure S9d shows representative UPS secondary electron edges (SEE) and Figure S9e the valence band maxima for pristine graphene and after successive treatments with the p-dopant. An increase in the work function is determined as the SEE shifts to lower binding energies. In contrast to n-doped samples, the Dirac point is not observed below the Fermi level. While from UPS we cannot ascertain that the Dirac point is above the Fermi level, the C 1s binding energy shift shown in Figure S9b is consistent with that shift, and is proof of transfer p-doping.

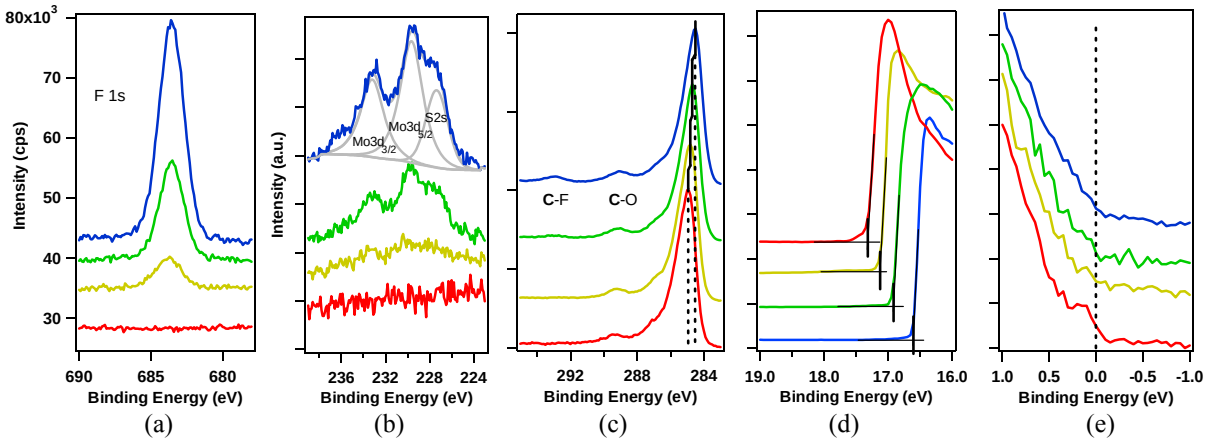

Fig S9 XPS and UPS comparison of pristine graphene (red) and after treatments with **2** (quick dips in 0.05 mM-yellow, 10 min in 5 mM-green, overnight in 5 mM-blue)**:** (a) F 1s, b) Mo 3d / S 2s region, c) C 1s region, with BE shift tracked for the main graphene peak, and **C**-F appearance after overnight treatment; the sample treated overnight has been fitted to show both atoms are present. (d) UPS secondary electron edge and (e) UPS valence band maximum region. Traces offset vertically for clarity in all graphs.

Table SIII Summary of GFET, XPS and UPS characterization after treatments with dopant **2**.

Result after treatment with ***2***	*1 s in 0.05 mM*	*10 min in 5 mM*	*12 h in 5 mM*
% Close-packed ML (XPS)	6 ± 2	26 ± 1	54 ± 5
$\varphi_{treated} - \varphi_{pristine}$ */eV (UPS SEE)*	0.23 ± 0.12	0.48 ± 0.13	0.71 ± 0.07
E_D-E_F */eV (from C1s)*	0.20 ± 0.10	0.40 ± 0.10	0.50 ± 0.10
n calculated from E_D-E_F */* cm^{-2}	(4 ± 2) x 10^{12}	(1.7 ± 0.4) x 10^{13}	(2.6 ± 0.5) x 10^{13}
Holes transferred per adsorbed dopant (XPS)	1.1 ± 0.6	1.0 ± 0.3	0.8 ± 0.2

Table SIV Binding energies (in eV) of main peaks in graphene treated with p-dopant **2**.

Treatment	*C 1s*	*F 1s*	*Mo* $3d_{5/2}$	*Si 2p*	*O 1s*
Pristine	285	-	-	104.3	533.5
Quick dips 0.05 mM	284.8	688.7	-	104.1	533.3
10 min, 5 mM	284.6	688.6	229.7	103.9	533.1
Overnight 5 mM	284.5	688.5	229.6	103.8	533.0

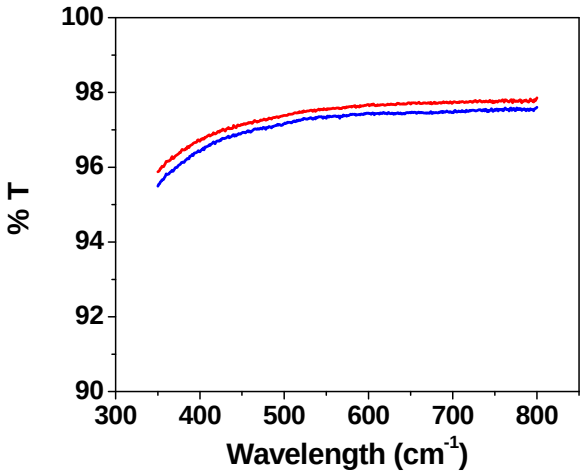

Fig S10 UV/Vis spectra for pristine graphene (red) and after 10 min treatment in **2** at 100 °C (blue). This abbreviated procedure gives similar WF changes and coverage as overnight treatment at r.t. according to photoemission spectroscopies.

11) Contribution of surface dipole to work function change after p-dopant treatment

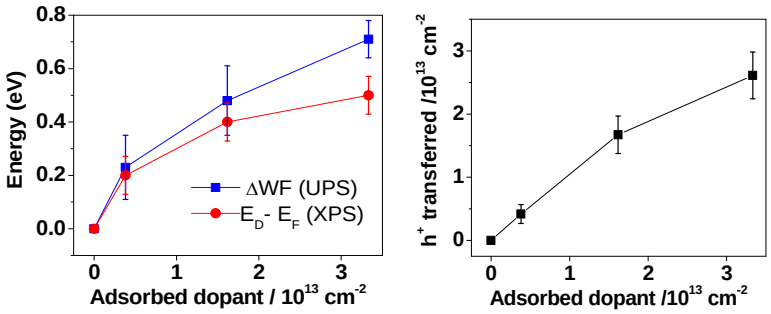

(a) (b)

Fig S11 (a) Work function change and shift of the Dirac point (with respect to Fermi level) with increasing deposited dopant **2**. (b) XPS-estimated density of holes transferred as a function of deposited dopant **2**.

Figure S11a shows that electron transfer from graphene to the dopant, depleting the population of the valence band in graphene (introduction of holes) does not account for all the observed changes in work function. We refer again to Equation 3 to explain the differences, where the surface dipole from the charges generated increases linearly with hole transfer. We see from the plot in Figure S11b that as the adsorbed dopant coverage increases, hole transfer becomes more difficult, and as Figure S11a makes clear, for each charge transferred, the surface dipole increases concomitantly.

Once more we noticed that the model reproduces our data well with certain assumptions: in Figure S12 we have assumed point charges with the positive charge at the graphene plane separated from the negative charge residing in the middle of the molecule, at vdW distance (C_{vdW} + F_{vdW})[12] from each other. Considering an average $\epsilon_r = 15$, the estimated surface dipole from Equation 3 in the main text reproduces fairly well the observed surface dipole for a given *n*. Table SV summarizes the observations and inferred results.

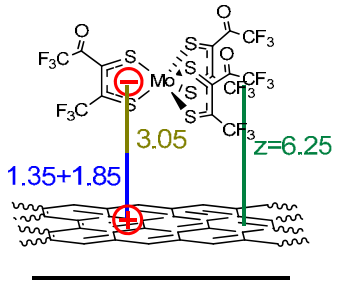

Fig S12 Schematic representation of surface dipole from hole transfer from **2**.

Table SV Estimation of surface dipole (SD) after treatment with p-dopant. The contribution of electron transfer from graphene to dopant to the WF shift, from which *n* was determined, is shown as well.

Treatment	*Observed* $\Delta\varphi_{ET}$ *(eV)*	*n from* $\Delta\phi_{ET}$ */ 10*^{13}	*Inferred* $\Delta\varphi_{SD}$ *(eV)*	$\mu_{SD} = q \times z$ *(C*m)*	*Estimated* $\Delta\varphi_{SD}$ *(eV)*
Quick dips 0.05 mM	*0.2 ± 0.1*	*0.4*	*0.03 ± 0.14*	*9.5x10*$^{-29}$	*0.03*
10 min 5 mM	*0.4 ± 0.1*	*1.7*	*0.08 ± 0.15*	*6.4x10*$^{-29}$	*0.13*
Overnight 5 mM	*0.5 ± 0.1*	*2.6*	*0.21 ± 0.10*	*1.1x10*$^{-28}$	*0.20*

12) Raman spectroscopy after p-dopant treatments

Figures S13 and S14 summarise the Raman observations under inert atmosphere. Again we compare our results with those of Das and coworkers acquired *in situ* with heavy electrical doping.[15] After treatments with the concentrated solution of the p-dopant, a significant decrease in the ratio of intensities of the 2D peak over the G peak is observed, consistent with strong doping. The 2D peak position suffers a shift to higher wavenumbers when using the concentrated solutions, in agreement with p-doping specifically. Finally, hole concentration is suggested to be on the order of 10^{13} for the 10 min and overnight treatments, based on the G peak position,[15] again in in accordance with the inferred values from photoemission spectroscopy.

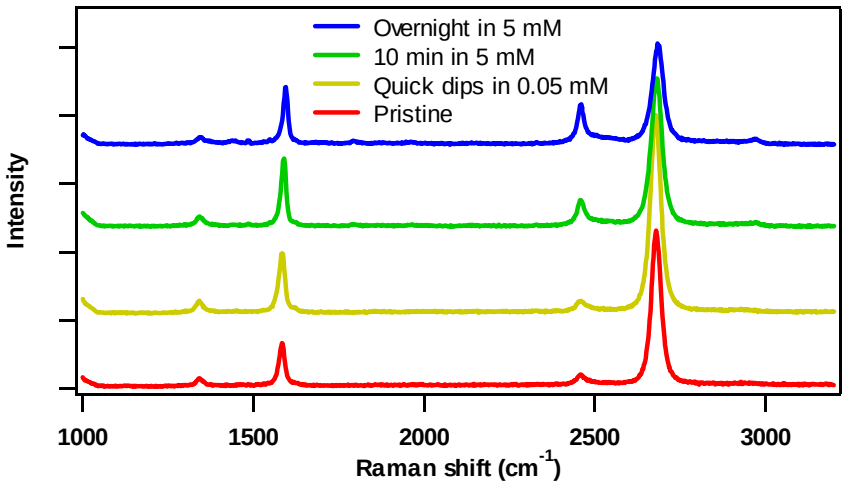

Fig S13 Raman spectra for graphene before and after successive p-doping treatments. Plots offset vertically for clarity.

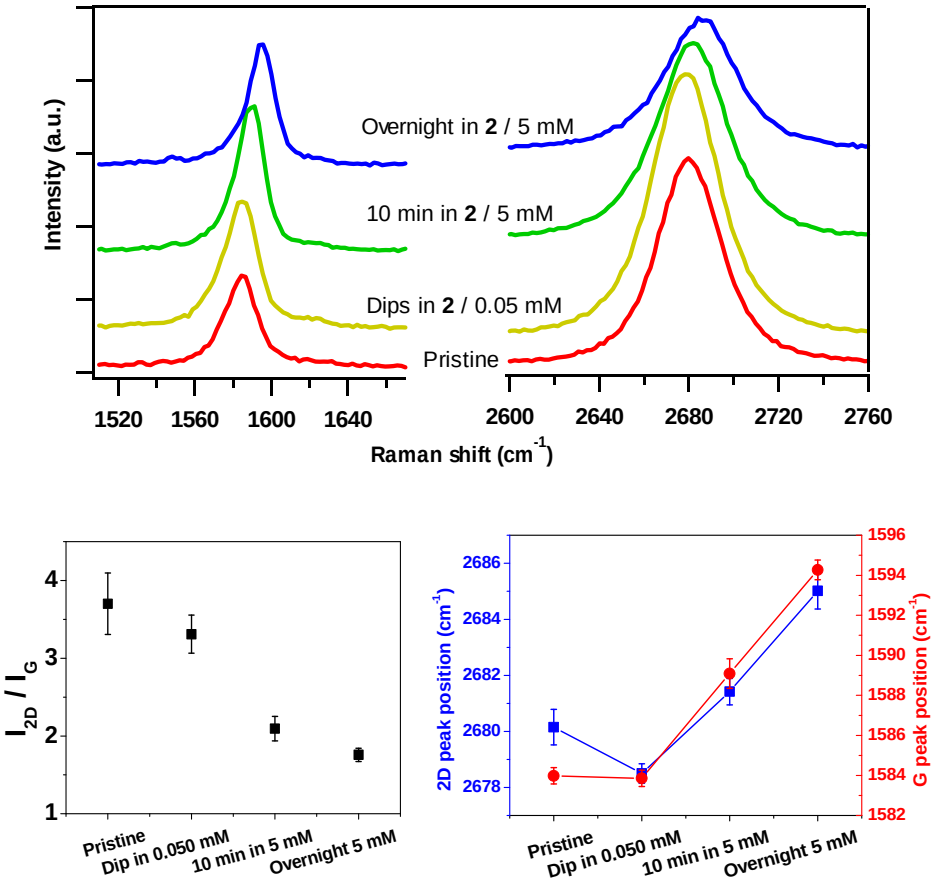

Fig S14 Zoom into the G and 2D Raman peaks for graphene before and after successive p-doping treatments, I_{2D}/I_G and 2D/G peak positions. Plots offset vertically for clarity.

*13) Comparison of results with **1**$_2$ and **2** to other treatments of graphene*

Table SVI. Comparison of the effects of various modifiers on the electronic properties of graphene.[a]

Graphene	Modifier	$\Delta\phi$ / eV[b]	$\Delta\phi_{CT}$ / eV[b]	n / cm^{-2}	Ref
CVD	Silane SAM under graphene	-0.3	–	2×10^{12} (e)[c]	6
CVD	Spin-coated MeO-DMBI	-0.7	–	1.9×10^{13} (e)[d]	16
CVD	Soaking in Cs_2CO_3	-0.85	~0.0[d]	–	17
rGO-CNT	Spunned Cs_2CO_3/250 °C	-1.7	–	–	18
Epitaxial	1 ML of Rb or Cs	–	-1.0	–	19
CVD	PEIE (polymer)	-0.8[e]	–	–	20
CVD	Submonolayer from **1**$_2$	-1.3	-0.7	$2\text{-}5\times10^{13}$(e) [b,d]	This work
CVD	Spin-coated $(CF_3SO_2)_2NH$	–	+0.7[d]	1×10^{14} (h)[f]	21
Epitaxial	Thin film MoO_3	+1.4	+0.7	1×10^{13} (h)[b]	14
Epitaxial	Thin film F_4-TCNQ	+1.0	+0.4	Dedoped[g]	22
Epitaxial	~ 1 ML of F_4-TCNQ	+1.3	+0.5	–	23
CVD	7 ML TCNQ/O_2	–	–	~10^{13} (h)[d]	24
CVD	Au NPs from $AuCl_3$	+0.5[h]	–		25
CVD	Treatment with HNO_3	+0.13[i]	–	9.4×10^{12}	26
CVD	Submonolayer from **2**	+0.7	+0.5	$1\text{-}3\times10^{13}$(h)[b,d]	This work

[a]Note that the mechanism by which the electronic changes are induced is not necessarily clear in every case, and that the work function differences for all CVD-graphene except Ref 6 and this work are determined relative to air-exposed graphene, which is generally found to be p-doped, while epitaxial graphene in its initial state is usually n-doped. Note also that we have described the shift of the WF due to (de)population of the graphene bands here in terms of charge transfer (CT) rather than ET, where CT is a more general term encompassing both integral electron transfer to / from the graphene and partial charge transfer (for example, such as that found in weak CT complexes). [b]From photoemission measurements. [c]From GFET measurements. [d]From Raman shifts. [e]From Kelvin probe in air. [f]From Hall measurements. [g]n-doping of 1×10^{13}cm^{-2} was reduced to 1.5×10^{11}cm^{-2}. [h]From scanning Kelvin probe in air. [i]GFET data for the as-transferred graphene showed p-doping corresponding to E_D-E_F~0.27 eV ($4.3\text{x}10^{12}$ cm^{-2}). Treatment with HNO_3 increases the doping further to 0.4 eV, which implies a total n=9.4×10^{12} holes cm^{-2}.

14) References for ESI

1 K. Moseley, J. W. Kang and P. M. Maitlis, *J. Chem. Soc. A*, 1970, **0**, 2875.

2 O. V. Gusev, L. I. Denisovich, M. G. Peterleitner, A. Z. Rubezhov, N. A. Ustynyuk and P. M. Maitlis, *J. Organomet. Chem.*, 1993, **452**, 219.

3 S. Guo, S. K. Mohapatra, A. Romanov, T. V. Timofeeva, K. I. Hardcastle, K. Yesudas, C. Risko, J.-L. Brédas, S. R. Marder and S. Barlow, *Chem. Eur. J.*, 2012, **18**, 14760.

4 M. Draganjac, E. Simhon, L. T. Chan, M. Kanatzidis, N. C. Baenziger and D. Coucouvanis, *Inorg. Chem.*, 1982, **21**, 3321.

5 Y. Shen, W. Qiu, Y. Xin and Y. Huang, *Synthesis*, 1984, **11**, 924.

6 J. Baltazar, H. Sojoudi, S. A. Paniagua, J. Kowalik, S. R. Marder, L. M. Tolbert, S. Graham and C. L. Henderson, *J. Phys. Chem. C*, 2012, **116**, 19095.

7 H. Sojoudi, J. Baltazar, C. Henderson and S. Graham, *J. Vac. Sci. Technol., B*, 2012, **30**, 041213.

8 C. K. Chan, W. Zhao, S. Barlow, S. Marder and A. Kahn, *Org. Electron.*, 2008, **9**, 575.

9 S. Guo, S. B. Kim, S. K. Mohapatra, Y. Qi, T. Sajoto, A. Kahn, S. R. Marder and S. Barlow, *Adv. Mater.*, 2012, **24**, 699.
10 B. W. D'Andrade, S. Datta, S. R. Forrest, P. Djurovich, E. Polikarpov and M. E. Thompson, *Org. Electron.*, 2005, **6**, 11.
11 S. K. Mohapatra, A. Romanov, G. Angles, T. V. Timofeeva, S. Barlow and S. R. Marder, *J. Organomet. Chem.*, 2012, **706–707**, 140.
12 C. E. Housecroft and A. G. Sharpe, *Inorganic Chemistry*, Pearson / Prentice Hall, Essex, UK, 2008.
13 L. Romaner, G. Heimel, C. Ambrosch-Draxl and E. Zojer, *Adv. Funct. Mater.*, 2008, **18**, 3999.
14 Z. Chen, I. Santoso, R. Wang, L. F. Xie, H. Y. Mao, H. Huang, Y. Z. Wang, X. Y. Gao, Z. K. Chen, D. Ma, A. T. S. Wee and W. Chen, *Appl. Phys. Lett.*, 2010, **96**, 213104.
15 A. Das, S. Pisana, B. Chakraborty, S. Piscanec, S. K. Saha, U. V. Waghmare, K. S. Novoselov, H. R. Krishnamurthy, A. K. Geim, A. C. Ferrari and A. K. Sood, *Nature Nanotech.*, 2008, **3**, 210.
16 P. Wei, N. Liu, H. R. Lee, E. Adijanto, L. Ci, B. D. Naab, J. Q. Zhong, J. Park, W. Chen, Y. Cui and Z. Bao, *Nano Lett.*, 2013.
17 K. C. Kwon, K. S. Choi, B. J. Kim, J.-L. Lee and S. Y. Kim, *J. Phys. Chem. C*, 2012, **116**, 26586.
18 J.-H. Huang, J.-H. Fang, C.-C. Liu and C.-W. Chu, *ACS Nano*, 2011, **5**, 6262.
19 S. Watcharinyanon, C. Virojanadara and L. I. Johansson, *Surf. Sci.*, 2011, **605**, 1918.
20 Y. Zhou, J. W. Shim, C. Fuentes-Hernandez, A. Sharma, K. A. Knauer, A. J. Giordano, S. R. Marder and B. Kippelen, *PCCP*, 2012, **14**, 12014.
21 S. Tongay, K. Berke, M. Lemaitre, Z. Nasrollahi, D. B. Tanner, A. F. Hebard and B. R. Appleton, *Nanotechnology*, 2011, **22**, 425701.
22 C. Coletti, C. Riedl, D. S. Lee, B. Krauss, L. Patthey, K. von Klitzing, J. H. Smet and U. Starke, *Phys. Rev. B*, 2010, **81**, 235401.
23 W. Chen, S. Chen, D. C. Qi, X. Y. Gao and A. T. S. Wee, *J. Am. Chem. Soc.*, 2007, **129**, 10418.
24 Y. Qi, U. Mazur and K. W. Hipps, *R. Soc. Chem. Adv.*, 2012, **2**, 10579.
25 Y. Shi, K. K. Kim, A. Reina, M. Hofmann, L.-J. Li and J. Kong, *ACS Nano*, 2010, **4**, 2689.
26 S. Bae, H. Kim, Y. Lee, X. Xu, J.-S. Park, Y. Zheng, J. Balakrishnan, T. Lei, H. Ri Kim, Y. I. Song, Y.-J. Kim, K. S. Kim, B. Ozyilmaz, J.-H. Ahn, B. H. Hong and S. Iijima, *Nature Nanotech.*, 2010, **5**, 574.